Bound states of the OH($^2\Pi$)–HCl complex on *ab initio* diabatic potentials

Gerrit C. Groenenboom, Anna V. Fishchuk,[a] and Ad van der Avoird[b]
Theoretical Chemistry, IMM, Radboud University Nijmegen, Heyendaalseweg 135, 6525 AJ Nijmegen, The Netherlands

(Received 3 February 2009; accepted 2 April 2009; published online 24 September 2009; publisher error corrected 12 October 2009)

The bound states of the open-shell OH($^2\Pi$)–HCl complex were calculated in four dimensions with a diabatic model using electronic states that correlate asymptotically with the ground and excited spin-orbit states of the OH($^2\Pi$) fragment and the ground state of the HCl fragment. The *ab initio* diabatic potentials and their analytic expansion applied in these calculations were obtained earlier by Wormer *et al.* [J. Chem. Phys. **122**, 244325 (2005)]. In addition to the four-dimensional calculations, we considered a (3+1)-dimensional model in which the intermolecular distance coordinate R is adiabatically separated from the remaining coordinates. Both models include the important spin-orbit coupling in the OH fragment. Energy levels and parity splittings were computed for a total angular momentum of $J=\frac{1}{2}$ and $\frac{3}{2}$; rotational constants and other spectroscopic parameters were extracted from these calculations. The vibrationally averaged geometry in the ground state of the complex is planar and this state is more or less localized near the minimum in the lowest adiabatic potential with binding energy $D_e=1123$ cm^{-1}; the dissociation energy D_0 with respect to OH($^2\Pi_{3/2}$) and HCl is found to be 685 cm^{-1}. The splitting between the $^2\Pi_{3/2}$ and $^2\Pi_{1/2}$ spin-orbit states of free OH is largely reduced by the anisotropic interaction with HCl through the off-diagonal diabatic coupling potential and these states are strongly mixed. Low lying rovibronic states that correlate with the OH($^2\Pi_{3/2}$) ground state were found at 14 cm^{-1} for total angular momentum projection quantum number $|\Omega|=\frac{3}{2}$ and 26 cm^{-1} for $|\Omega|=\frac{1}{2}$, relative to the ground state with $|\Omega|=\frac{1}{2}$. The OH–HCl stretch fundamental frequency equals to 93.6 cm^{-1}, the lowest bend excited states (involving a coupled bend motion of both fragments) were found in the region of 150–160 cm^{-1} above the ground state. Especially in the excited states important nonadiabatic effects are observed that involve both of the asymptotically degenerate adiabatic electronic states. In some of these excited states the vibrationally averaged geometry is nonplanar. © *2009 American Institute of Physics*. [doi:10.1063/1.3123426]

I. INTRODUCTION

It is well known that hydroxyl radicals play a very important role in atmospheric chemistry as well as in combustion processes.[1,2] Due to its high reactivity the OH radical is easily involved in chemical interactions with hydrogen halides, which lead to release of halogens in their active atomic state. In particular, the reaction OH+HCl→H_2O+Cl is a primary source of atomic chlorine in the atmosphere. A number of kinetic experiments have been carried out on the OH+HCl system,[3–10] where the temperature-dependent rate constants were measured over a wide temperature range. Crossed molecular beam experiments have been performed also, including the measurement of steric effects depending on the orientation of the incoming OH radicals. These experiments produced inelastic OH–HCl scattering cross sections, but reaction products could not be observed.[11,12]

There are also a number of theoretical studies for the OH+HCl→H_2O+Cl reaction[13–18] that concentrated mostly on the region of the reaction transition state. By employing second-order Møller–Plesset (MP2) calculations, Yu and Nyman[15] found that the weakly bound OH–HCl complex formed in the entrance channel of the reaction has a planar geometry and that an early saddle point occurs for a nonplanar geometry. Probably the most accurate *ab initio* calculations for the (nonreactive) OH–HCl intermolecular potential energy surfaces (PESs) were carried out by Wormer *et al.*[18] They used the partially spin restricted coupled-cluster-singles-doubles plus noniterative triples [RCCSD(T)] method for the lowest potential and the multireference configuration interaction method for the energy difference between the first excited state potential and the ground state potential. They also computed the adiabatic mixing angle that allowed them to obtain suitable diabatic potentials from the adiabatic *ab initio* potentials, and they made the analytic expansion of the diabatic potentials that we used in bound state calculations.

Infrared spectroscopic measurements of the intermolecular bend and spin-orbit states in the OH stretch overtone region were made by Marshall *et al.*[19,20] and Marshall and Lester[21] for other OH-diatom complexes, namely, OH–N_2 and OH–CO, and for the OH-acetylene complex. Spectra of the latter complex were also measured in the acetylenic asymmetric CH stretch region. These authors presented a

[a]Electronic mail: anaf@list.ru.
[b]Electronic mail: a.vanderavoird@theochem.ru.nl.

theoretical analysis of the OH–N_2 and OH–CO spectra with the use of a model that includes the $\omega=\pm\frac{3}{2}$ spin-orbit ground state of the OH($^2\Pi$) fragment and the bends of both monomers. They also carried out model calculations with the use of an intermolecular potential consisting of the OH dipole-N_2 (or CO) quadrupole interaction. The OH-acetylene spectra were interpreted with the aid of a rigid T-shaped model.

Here, we present, analyze, and compare the results obtained from two different models for the bound states of the OH–HCl complex. The first four-dimensional (4D) model treats all intermolecular coordinates simultaneously and the second (3+1)D model makes an adiabatic separation between the coordinate R, the distance between the OH and HCl centers of mass, and the remaining coordinates. All calculations involve both the ground $\omega=\pm\frac{3}{2}$ and excited $\omega=\pm\frac{1}{2}$ spin-orbit components of the OH($^2\Pi$) monomer and are based on *ab initio* diabatic potentials.[18]

II. THEORY

The OH–HCl complex is considered as a rotating dimer consisting of two rigid monomers denoted as monomer A, which stands for the OH radical, and monomer B, which is the HCl molecule. The O–H bond length r_{OH} is fixed at $1.950a_0$.[22,23] The H–Cl bond length $r_{\mathrm{HCl}}=2.4094a_0$ corresponds to the equilibrium distance.[24] The Hamiltonian of the complex is expressed in Jacobi coordinates as (in atomic units with $\hbar=1$)

$$\hat{H}=\hat{H}_{\mathrm{OH}}+\hat{H}_{\mathrm{HCl}}-\frac{1}{2\mu_{AB}R}\frac{\partial^2}{\partial R^2}R+\frac{\hat{\mathbf{J}}^2+\hat{\mathbf{j}}_{A,B}^2-(\hat{j}_{-,AB}^{(\mathrm{DF})}\hat{J}_{-}^{(\mathrm{DF})}+\hat{j}_{+,AB}^{(\mathrm{DF})}\hat{J}_{+}^{(\mathrm{DF})}+2\hat{j}_{z,AB}^{(\mathrm{DF})}\hat{J}_{z}^{(\mathrm{DF})})}{2\mu_{AB}R^2}+\hat{V}(R,\theta_A,\theta_B,\phi). \tag{1}$$

It consists of the monomer Hamiltonians

$$\hat{H}_{\mathrm{OH}}=B_{0_{\mathrm{OH}}}(\hat{\mathbf{j}}_A^2-\hat{j}_{z,A}^{2(\mathrm{MF})}+\hat{\mathbf{S}}^2-\hat{S}_z^{2(\mathrm{MF})}-\hat{S}_{+}^{(\mathrm{MF})}\hat{j}_{+,A}^{(\mathrm{MF})}-\hat{S}_{-}^{(\mathrm{MF})}\hat{j}_{-,A}^{(\mathrm{MF})})+\hat{H}_{\Lambda\mathrm{D}}+A_0\hat{L}_z^{(\mathrm{MF})}\hat{S}_z^{(\mathrm{MF})} \tag{2}$$

and

$$\hat{H}_{\mathrm{HCl}}=B_{0_{\mathrm{HCl}}}\hat{\mathbf{j}}_B^2, \tag{3}$$

the radial kinetic energy operator for the relative motion of the monomers, the kinetic energy operator for the end-over-end rotation of the complex expressed in body-fixed coordinates, and the potential energy operator

$$\hat{V}(R,\theta_A,\theta_B,\phi)=\sum_{\Lambda',\Lambda}|\Lambda'\rangle V_{\Lambda',\Lambda}(R,\theta_A,\theta_B,\phi)\langle\Lambda|. \tag{4}$$

The quantum number Λ is the projection of the electronic orbital angular momentum of the open-shell OH radical on the OH axis; the potential energy operator in Eq. (4) couples the diabatic states of the complex with $\Lambda=\pm1$ that correlate with the corresponding components of the $^2\Pi$ state of the OH radical. Other quantities appearing in the Hamiltonian are the reduced mass $\mu_{AB}=m_Am_B/(m_A+m_B)$ with $m_A=m_{\mathrm{H}}+m_{\mathrm{O}}$ and $m_B=m_{\mathrm{H}}+m_{\mathrm{Cl}}$, where m_{H}, m_{O}, and m_{Cl} are the atomic masses, and the angular momentum operators $\hat{\mathbf{j}}_A$, $\hat{\mathbf{j}}_B$, and $\hat{\mathbf{J}}$. The operator $\hat{\mathbf{J}}$ represents the total angular momentum of the system, $\hat{\mathbf{j}}_A$ and $\hat{\mathbf{j}}_B$ are the monomer angular momenta, and $\hat{\mathbf{j}}_{AB}=\hat{\mathbf{j}}_A+\hat{\mathbf{j}}_B$.

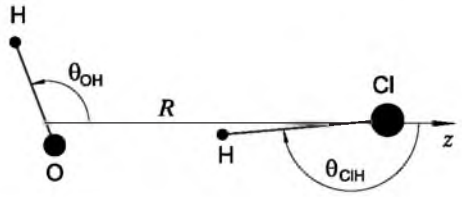

FIG. 1. Hydrogen-bonded equilibrium geometry of OH–HCl in the lower adiabatic potential V_1 with $\theta_{\mathrm{OH}}=110.7°$, $\theta_{\mathrm{ClH}}=176.4°$, $\phi=180°$, and $R_e=6.36a_0$.

A two-angle embedded dimer-fixed (DF) frame is defined with its z-axis parallel to the vector $\mathbf{R}$, which points from the center of mass of the OH radical to the center of mass of the HCl molecule. Two monomer-fixed (MF) frames have their z-axis along the molecular axes of OH and HCl. The coordinates (β,α) are the space fixed (SF) polar angles of $\mathbf{R}$, (θ_A,ϕ_A) are the polar angles of the vector $\mathbf{r}_{\mathrm{OH}}$ (pointing from O to H) with respect to the DF frame, and (θ_B,ϕ_B) are the polar angles of $\mathbf{r}_{\mathrm{HCl}}$ pointing from Cl to H, also in the DF frame. The dihedral angle ϕ is defined as $\phi=\phi_A-\phi_B$. See Fig. 1 for an illustration of the coordinates.

The dimer frame fixed and monomer frame fixed components of the angular momentum operators, labeled by the superscripts DF and MF, must be distinguished because they act differently on the angular coordinates and on the basis functions (defined below). This is reflected by the action of the shift operators, which are defined in the usual way except those that act on the angles used to define their frame.[25] The latter are given by

$$\hat{J}_{\pm}^{(\mathrm{DF})}=\hat{J}_x^{(\mathrm{DF})}\mp i\hat{J}_y^{(\mathrm{DF})},$$

$$\hat{j}_{\pm,A}^{(\mathrm{MF})}=\hat{j}_{x,A}^{(\mathrm{MF})}\mp i\hat{j}_{y,A}^{(\mathrm{MF})}, \tag{5}$$

$$\hat{j}_{\pm,B}^{(\mathrm{MF})}=\hat{j}_{x,B}^{(\mathrm{MF})}\mp i\hat{j}_{y,B}^{(\mathrm{MF})}.$$

The angular momentum operators $\hat{\mathbf{J}}^2$, $\hat{\mathbf{j}}_A^2$, $\hat{\mathbf{j}}_B^2$, $\hat{\mathbf{j}}_{AB}^2$, and $\hat{\mathbf{S}}^2$ are frame independent.

In the OH monomer Hamiltonian, $\hat{\mathbf{S}}$ represents the spin operator. The spin-orbit coupling constant equals $A_0=-139.21\ \mathrm{cm}^{-1}$ and the ground state rotational constants of OH and HCl are $B_{0_{\mathrm{OH}}}=18.5487\ \mathrm{cm}^{-1}$ and $B_{0_{\mathrm{HCl}}}=10.440\ 19\ \mathrm{cm}^{-1}$.[26] The Λ-type doubling term of OH is

$$\hat{H}_{\Lambda D}=\hat{\Lambda}_{-}^{2(\mathrm{MF})}\left[-\left(\frac{p}{2}+q\right)\hat{S}_{+}^{(\mathrm{MF})}\hat{j}_{-,A}^{(\mathrm{MF})}+\frac{q}{2}\hat{j}_{-,A}^{2(\mathrm{MF})}\right]+\hat{\Lambda}_{+}^{2(\mathrm{MF})}\left[-\left(\frac{p}{2}+q\right)\hat{S}_{-}^{(\mathrm{MF})}\hat{j}_{+,A}^{(\mathrm{MF})}+\frac{q}{2}\hat{j}_{+,A}^{2(\mathrm{MF})}\right] \tag{6}$$

with the parameters $p=0.235$ cm^{-1} and $q=-0.0391$ cm^{-1}.[26] The operator $\hat{\Lambda}_{-}^{2(\mathrm{MF})}=|-1\rangle\langle 1|$ couples the two components of the OH($^2\Pi$) state and $\hat{\Lambda}_{+}^{2(\mathrm{MF})}=\hat{\Lambda}_{-}^{2(\mathrm{MF})\dagger}$ is its Hermitian conjugate.

The diabatic potentials $V_{\Lambda',\Lambda}(R,\theta_A,\theta_B,\phi)$ in Eq. (4) are the OH–HCl interaction potentials for the diabatic electronic states $|\Lambda\rangle$ with $\Lambda=\pm 1$ and the diabatic PESs form a 2×2 matrix. They are related to the *ab initio* adiabatic PESs by

$$V_{-1,-1}=V_{1,1}=\tfrac{1}{2}(V_1+V_2), \tag{7}$$

$$V_{-1,1}=V_{1,-1}^{*}=\tfrac{1}{2}(V_2-V_1)\exp(-2i\gamma), \tag{8}$$

where γ represents the mixing angle depending on the same variables as the potentials. The adiabatic PESs V_1 and V_2 are the energies of the ground and the first excited electronic states, which become degenerate when the OH($^2\Pi$) and HCl fragments are separated. In our calculations it was convenient to use the expansion of the diabatic potentials from Ref. 18,

$$\begin{aligned}V_{\Lambda,\Lambda'}(R,\theta_A,\theta_B,\phi)&=\sum_{L_A L_B L} v_{L_A L_B L}^{\Lambda\Lambda'}(R)\sum_{M}\langle L_A,M;L_B,-M|L,0\rangle\\&\times D_{M,\Lambda'-\Lambda}^{L_A}(\phi_A,\theta_A,0)^{*}C_{L_B,-M}(\theta_B,\phi_B),\end{aligned} \tag{9}$$

where $D_{MK}^{L}(\phi,\theta,\psi)$ are Wigner D-functions, $C_{LM}(\theta,\phi)$ are Racah normalized spherical harmonic functions, $\langle l,m;l',m'|L,M\rangle$ are Clebsch–Gordan coefficients,[27] and $v_{L_A L_B L}^{\Lambda\Lambda'}(R)$ are the R-dependent expansion coefficients.

The basis in which we carry out the bound state calculations for the OH–HCl complex is similar to the basis used by Offer and van Hemert[28] and Offer *et al.*[29] in coupled channel calculations for inelastic OH–H_2 collisions. This basis is called diabatic because its electronic part $|S,\Sigma\rangle|\Lambda\rangle$ corresponds to the diabatic states which define the diabatic potentials. The diabatic basis for the bound state (or scattering) calculations includes, however, more functions. The rotronic part of the diabatic basis function is given by the electronic basis functions and a coupled product of symmetric rotor functions (Wigner D-functions) and spherical harmonics $Y_{jm}(\theta,\phi)$,

$$\begin{aligned}|\Lambda,\omega_A,j_A,j_B,j_{AB},\Omega\rangle&=\left[\frac{(2J+1)(2j_A+1)}{16\pi^2}\right]^{1/2}|S,\Sigma\rangle|\Lambda\rangle\sum_{m_A m_B}\\&\times[D_{m_A\omega_A}^{(j_A)}(\phi_A,\theta_A,0)^{*}Y_{j_B m_B}(\theta_B,\phi_B)\langle j_A m_A;j_B m_B|j_{AB}\Omega\rangle]\\&\times D_{M\Omega}^{(J)}(\alpha,\beta,0)^{*}.\end{aligned} \tag{10}$$

Here, $\omega_A=\Sigma+\Lambda$ is the projection of the $\hat{\mathbf{j}}_A^{(\mathrm{MF})}$ operator on the OH axis and Σ is the spin projection. Ω is a nearly good quantum number, which represents the projection of the total angular momentum operator $\hat{\mathbf{J}}$ on the intermolecular axis along the vector $\mathbf{R}$, which is the z-axis of the DF frame. The summation indices m_A and m_B are the projections of the angular momentum operators $\hat{\mathbf{j}}_A^{(\mathrm{DF})}$ and $\hat{\mathbf{j}}_B^{(\mathrm{DF})}$ onto the intermolecular axis, respectively. The exact quantum number M is the projection of the operator $\hat{\mathbf{J}}$ onto the z-axis of the SF frame. M, as well as the exact quantum numbers J and S, was omitted from the short notation on the left hand side.

The full diabatic basis functions including the radial part are written in the following form:

$$|n,\Lambda,\omega_A,j_A,j_B,j_{AB},\Omega\rangle=R^{-1}\Phi_n(R)|\Lambda,\omega_A,j_A,j_B,j_{AB},\Omega\rangle, \tag{11}$$

where $|n\rangle=R^{-1}\Phi_n(R)$ is a radial basis function and $\Phi_n(R)$ is a contracted sinc-DVR (discrete variable representation) function.[30] The radial reference potential $V^{\mathrm{ref}}(R)$ used to generate this radial basis is obtained from a radial cut $V^{\mathrm{cut}}(R)$ of the lowest adiabatic potential V_1 through the global minimum ($\theta_A=110.7°$, $\theta_B=176.4°$, and $\phi=180°$). By scaling the radial coordinate R so that $V^{\mathrm{ref}}(R)=V^{\mathrm{cut}}(R/\alpha)$ we optimized the radial basis through varying α. The optimum value was $\alpha=0.98$. In this optimization procedure we checked not only the ground state but also the lowest five excited states.

In addition to J, M, and S, the parity p of the states under the inversion $\hat{i}$ is a good quantum number. The effect of inversion on the basis is

$$\hat{i}|n,\Lambda,\omega_A,j_A,j_B,j_{AB},\Omega\rangle=(-1)^{S+j_A+j_B+j_{AB}+J}|n,-\Lambda,-\omega_A,j_A,j_B,j_{AB},-\Omega\rangle. \tag{12}$$

Hence, we construct a parity-adapted basis in the following way:

$$\begin{aligned}|n,\Lambda,\omega_A,j_A,j_B,j_{AB},\Omega,p\rangle&=\frac{1}{\sqrt{2}}[|n,\Lambda,\omega_A,j_A,j_B,j_{AB},\Omega\rangle\\&+p(-1)^{S+j_A+j_B+j_{AB}+J}|n,-\Lambda,-\omega_A,j_A,j_B,j_{AB},-\Omega\rangle],\end{aligned} \tag{13}$$

in which we restrict ourselves to positive values of Ω. It is customary to use the spectroscopic parity $\epsilon=p(-1)^{J-S}$ rather than the total parity p. States with parities $\epsilon=1$ (even) and $\epsilon=-1$ (odd) are denoted with e and f, respectively.

The form of a matrix element of the potential, Eq. (4), in the primitive diabatic basis is

$$\langle n',\Sigma',\Lambda',\omega_A',j_A',j_B',j_{AB}',\Omega'|\hat{V}(R,\theta_A,\theta_B,\phi)|n,\Sigma,\Lambda,\omega_A,j_A,j_B,j_{AB},\Omega\rangle$$
$$= \delta_{\Sigma',\Sigma}\delta_{\Omega',\Omega}\sum_{L_A,L_B,L}(-1)^{L_A-L_B+j_A-j_B+j_{AB}-L-\omega_A'-\Omega}\langle n'|v_{L_AL_BL}^{\Lambda',\Lambda}(R)|n\rangle$$
$$\times[(2L+1)(2j_A'+1)(2j_A+1)(2j_B'+1)(2j_B+1)(2j_{AB}'+1)(2j_{AB}+1)]^{1/2}$$
$$\times\begin{pmatrix} j_A' & L_A & j_A \\ -\omega_A' & \Lambda'-\Lambda & \omega_A\end{pmatrix}\begin{pmatrix} j_B' & L_B & j_B \\ 0 & 0 & 0\end{pmatrix}\begin{pmatrix} j_{AB}' & L & j_{AB} \\ -\Omega & 0 & \Omega\end{pmatrix}\begin{Bmatrix} j_A' & L_A & j_A \\ j_B' & L_B & j_B \\ j_{AB}' & L & j_{AB}\end{Bmatrix} \quad (14)$$

in terms of 3-j and 9-j symbols. In the evaluation of the matrix elements of other terms in the Hamiltonian we used the well known properties of the angular momentum operators. Complete formulas are presented in Ref. 31.

III. BOUND STATE CALCULATIONS

In addition to the full 4D calculations involving all intermolecular coordinates we applied an approximate (3+1)D model. The results from this (3+1)D model are useful in the interpretation of the 4D results. In all calculations we used the diabatic PESs computed earlier by Wormer *et al.*[18] The data needed to compute the expansion coefficients $v_{L_AL_BL}^{\Lambda\Lambda'}(R)$ of these potentials for arbitrary values of R, see Eq. (9), are obtained from Ref. 18.

A. 4D calculations

The calculations were carried out in four dimensions with the coordinates R,θ_A,θ_B,ϕ for two values of the total angular momentum, $J=\frac{1}{2}$ and $\frac{3}{2}$. The 4D bound states of the complex were obtained by solving the Hamiltonian matrix eigenvalue problem with the Davidson[32] algorithm with convergence to at least 10^{-2} cm^{-1}. The angular basis is truncated at $j_{A_{\max}}=9.5$, $j_{B_{\max}}=11$ and the radial basis is truncated at $n_{\max}=15$. The angular basis size is similar to that used in bound state calculations for the water dimer by Groenenboom *et al.*, cf. Table III in Ref. 33. The OH–HCl and H_2O–H_2O systems are similar in the potential anisotropy and well depth. In order to check the convergence of the basis we carried out 4D calculations with $j_{A_{\max}}=7.5$, $j_{B_{\max}}=8$, and a radial basis with $n_{\max}=15$ as well as three-dimensional (3D) calculations for fixed $R=6.4a_0$ with $J=\frac{1}{2}$. In the 4D calculations, the ground state energy for the smaller angular basis is equal to -721.09 cm^{-1}, while the corresponding energy for the basis with $j_{A_{\max}}=9.5$ and $j_{B_{\max}}=11$ used in the calculations is -723.12 cm^{-1}. In the 3D calculations for $R=6.4a_0$ we observed that increasing $j_{A_{\max}}$ from 8.5 to 9.5 lowers the ground state energy by only 0.004 cm^{-1}, while increasing $j_{B_{\max}}$ from 10 to 11 lowers it by nearly 0.2 cm^{-1}. The convergence is considerably better for quantities formed from energy differences such as vibrational excitation energies, rotational constants, parity splittings, etc.

B. (3+1)D calculations

For closed-shell systems the method explained in this section is referred to as Born–Oppenheimer angular-radial separation[34] or sometimes as the adiabatic bender (AB) approximation.[35] Here we apply a similar adiabatic separation to the angular and electronic coordinates, on the one hand, and the distance R on the other. The method consists of two steps. First, the AB potentials were obtained by a series of 3D calculations with R fixed at values ranging from 4.8 to $15.0a_0$ in steps of $0.1a_0$ for $J=\frac{1}{2}$ and $J=\frac{3}{2}$. The 3D calculations are carried out with almost the same Hamiltonian (1) as the 4D calculations except that the radial kinetic energy operator is omitted and the radial coordinate R is fixed. The rotronic basis used is the same as in the 4D model, see Eq. (10). The R-dependence of the energy levels from the 3D calculations is shown in Fig. 2, which contains also the levels from the full 4D calculations. The curves in Fig. 2 are the AB potentials. When curves corresponding to the different values of J nearly coincide, they belong to the same $|\Omega|$ value. In the second step of the (3+1)D model, each AB potential was used to calculate stretch vibrational energy levels for the complex. The required one-dimensional (1D) calculations were made with the sinc-DVR method.[30] The AB curves asymptotically correlate with the molecular states of the OH and HCl molecules, therefore, these curves can be labeled with the quantum numbers of OH($^2\Pi$) and HCl. One

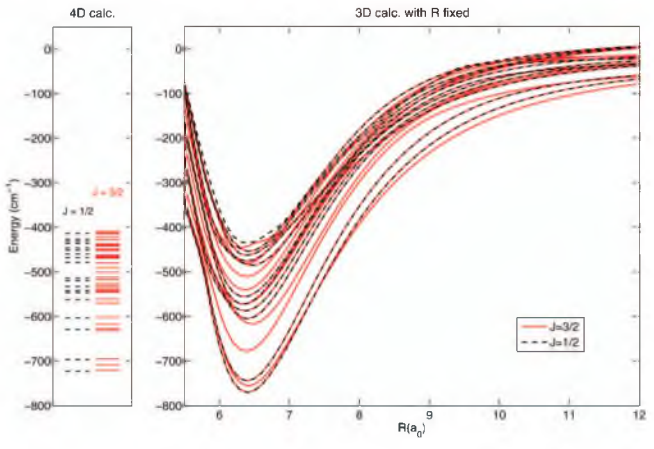

FIG. 2. The AB potentials in comparison with the 4D calculated energy levels both of e parity.

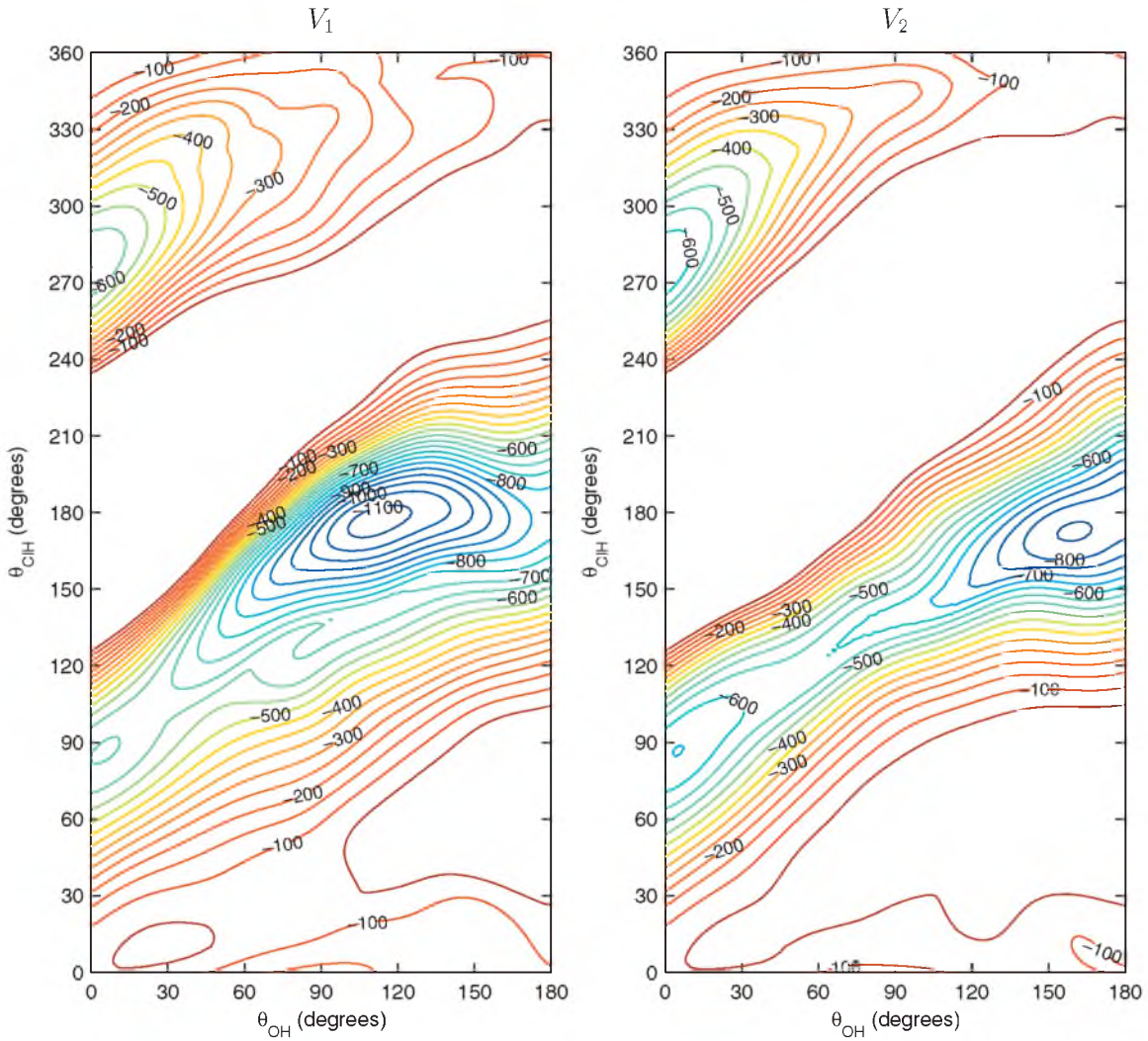

FIG. 3. Adiabatic potentials V_1 and V_2 in cm^{-1} for $\phi=180°$ and optimized R. The range of the angle θ_{ClH} has been extended up to 360° in order to cover all planar geometries. The upper half of the figure for $180° \leq \theta_{ClH} \leq 360°$ corresponds to the usual range of $180° \geq \theta_{ClH} \geq 0°$ with $\phi=0°$.

has to keep in mind, however, that the character of the wave functions rapidly changes where the curves have avoided crossings.

IV. RESULTS AND DISCUSSION

Section IV A describes the data computed and the definition of the parameters used to assign the bound states. Section IV B proceeds with the characterization of the bound states and the analysis of the effects that cause their properties.

A. Assignment of bound states

For the interpretation of the bound states it is useful to consider first the relevant potential surfaces of OH–HCl computed in Ref. 18. Figure 3 shows the adiabatic intermolecular potentials corresponding to the ground (V_1) and excited (V_2) states. The global minimum in the lower potential, see Fig. 1, has a depth $D_e=1123$ cm^{-1} and is located at $\theta_{OH}=110.7°$, $\theta_{ClH}=176.4°$, and dihedral angle $\phi=180°$ with $R_e=6.36a_0$. The global minimum of the V_2 potential has a smaller D_e value of 857 cm^{-1} and it is located at $\theta_{OH}=159.8°$, $\theta_{ClH}=172.5°$, $\phi=180°$, and $R_e=6.55a_0$. The global minimum of the V_1 potential represents a hydrogen-bonded structure with HCl being the donor and OH the acceptor. The global minimum of the V_2 potential in comparison with the V_1 potential is shifted toward a larger value of the θ_{OH} coordinate, approaching the linear geometry. There is also a local minimum in both potential surfaces, V_1 and V_2. These local minima represent a hydrogen-bonded structure as well, but OH is now the donor and HCl is the acceptor. The local minima are almost identical for the two potentials. The local minimum in the V_1 potential is located at $\theta_{OH}=5.5°$, $\theta_{ClH}=86.9°$, and $\phi=180°$ with $R_e=6.65a_0$ and has $D_e=655$ cm^{-1}; the V_2 local minimum has $D_e=651$ cm^{-1} with $R_e=6.65a_0$ and is located at $\theta_{OH}=4.9°$ and $\theta_{ClH}=86.7°$.

Table I presents the energies and corresponding quantum numbers for $|\Omega|=\frac{1}{2}$ from the two types of calculations, 4D and (3+1)D, for total angular momentum quantum number $J=\frac{1}{2}$. The stretch vibrational quantum number v_s is assigned to the 4D results by analyzing the populations of the radial basis functions $\Phi_n(R)$. If a basis function with a certain value of n occurs in the bound state with probability (population) larger than or equal to 50%, we assign the quantum number $v_s=n$ to this bound state. If the population is less than 50%

TABLE I. Energies of lowest bound states of e parity and rotational constants B_v in cm^{-1} from 4D and (3+1)D calculations for $|\Omega|=\frac{1}{2}$. The geometry labels pl and npl refer to planar and nonplanar structures; the approximate spin-orbit quantum numbers $\bar{\omega}_A, \langle|\omega_A|\rangle, \bar{\Lambda}$ are explained in the text; v_s, $v_{b_{OH}}$, and $v_{b_{HCl}}$ are approximate quantum numbers for the stretch, OH bend, and HCl bend modes, respectively. The (3+1)D results are labeled with $\sharp$ and η numbers the AB potentials from which they were obtained.

State	$E_{J=1/2}$	Geometry	$\bar{\omega}_A$	$\langle\|\omega_A\|\rangle$	$\bar{\Lambda}$	v_s	$v_{b_{OH}}$	$v_{b_{HCl}}$	B_v	$E^{\sharp}_{J=1/2}$	$(\eta,v_s)^{\sharp}$	$B^{\sharp}_v$
1	−723.12	pl	−0.51	1.16	−0.21	0	0	0	0.1232	−721.65	0,0	0.1255
2	−697.17	pl	0.38	1.13	0.09	0	0	0	0.1255	−695.74	1,0	0.1258
3	−629.54	pl	−0.55	1.17	−0.24	1	0	0	0.1194	−628.51	0,1	0.1219
4	−603.58	pl	0.40	1.14	0.10	1	0	0	0.1215	−602.69	1,1	0.1223
5	−562.53	pl	−0.40	1.20	−0.19	0	1	0	0.1248	−561.77	2,0	0.1267
6	−547.03	pl	−0.14	1.17	−0.09	0	1	0	0.1246	−545.77	3,0	0.1277
7	−542.08	pl	−0.55	1.19	−0.26	2*	0	0	0.1135	−543.42	0,2	0.1184
8	−532.94	npl	0.13	1.07	0.06	0	1	0	0.1265	−526.96	4,0	0.1275
9	−519.75	npl	0.24	1.09	0.01	0	⋯	⋯	0.1244	−512.25	5,0	0.1270
10	−514.46	pl	0.29	1.08	0.01	2*	0	0	0.1206	−517.85	1,2	0.1192
11	−479.03	pl	−0.39	1.22	−0.20	1	1	0	0.1203	−479.83	2,1	0.1250
12	−468.24	npl	−0.25	1.18	−0.13	1	⋯	⋯	0.1248	−464.62	3,1	0.1251
13	−460.03	npl	−0.54	1.20	−0.27	⋯	⋯	⋯	0.1146	−466.74	0,3	0.1153
14	−451.77	npl	0.31	1.13	0.03	1	⋯	⋯	0.1226	−440.58	4,1	0.1231
15	−451.46	npl	−0.11	1.08	−0.07	1*	⋯	⋯	0.1316	−428.64	5,1	0.1228
16	−446.23	pl	−0.74	1.27	−0.43	0	0	1	0.1205	−449.27	6,0	0.1246
17	−436.50	pl	0.58	1.18	0.24	0*	2	0	0.1181	−437.59	7,0	0.1259
18	−431.26	pl	0.40	1.16	0.16	0*	⋯	⋯	0.1184	−441.58	1,3	0.1164
19	−426.56	pl	−0.80	1.24	−0.51	0	⋯	⋯	0.1240	−422.37	8,0	0.1248
20	−413.52	pl	0.34	1.21	0.15	0	⋯	⋯	0.1238	−412.95	9,0	0.1246

but still has a substantial value (e.g., 40%), then we mark the quantum number with a * and call it mixed. If the populations are almost equally divided over different values of the stretch quantum number, we put the sign ⋯.

The quantum number ω_A, the projection of the electronic angular momentum on the OH axis, is not a good quantum number and according to the population analysis is rather mixed. The expectation value of ω_A cannot be used to characterize the electronic character of the eigenstates, since they are parity adapted and the components with $\pm\omega_A$ occur with equal weights. This happens already in free OH, where the expectation value $\langle\omega_A\rangle=\langle\hat{J}^{(\mathrm{MF})}_{z,A}\rangle$ cannot be used to distinguish the ground state with $\omega_A=\pm\frac{3}{2}$ and the excited spin-orbit state with $\omega_A=\pm\frac{1}{2}$ because also the eigenstates of OH are parity adapted and the expectation value $\langle\omega_A\rangle$ equals to 0 for both states. A possible way to distinguish the ground and spin-orbit excited states of OH is to consider only the components with positive ω_A in the parity-adapted states, or, equivalently, one may compute the expectation values $\bar{\omega}_A$ of the product operator $\hat{L}_z\hat{J}^{(\mathrm{MF})}_{z,A}$, where the role of the electronic orbital angular momentum operator $\hat{L}_z$ with eigenvalues $\Lambda=\pm1$ is only to compensate for the sign of ω_A. Another possibility is to compute the expectation value $\langle|\omega_A|\rangle=\langle|\hat{J}^{(\mathrm{MF})}_{z,A}|\rangle$. In the case of free OH these two options are equivalent, they both produce the ω_A value of $\frac{3}{2}$ for the ground state and $\frac{1}{2}$ for the excited state. In the OH–HCl complex the OH substates with $\omega_A=-\frac{3}{2},-\frac{1}{2},\frac{1}{2},\frac{3}{2}$ are all mixed. A further complication is that for the OH–HCl complex yet another projection quantum number appears, namely, Ω, which represents the total angular momentum projection on the DF z-axis. The parity-adapted states of OH–HCl are equal mixtures of the basis functions $|\Lambda,\omega_A,\Omega\rangle$ and $|-\Lambda,-\omega_A,-\Omega\rangle$, see Eq. (13). By analogy with the free OH molecule, where we considered only the components with positive ω_A, we now consider only the $\Omega>0$ components of the parity-adapted states in the analysis and compute the average value $\bar{\omega}_A$ from these components only. The expectation value $\langle|\omega_A|\rangle=\langle|\hat{J}^{(\mathrm{MF})}_{z,A}|\rangle$ is defined in the usual way as above. In Tables I and II we present both quantities which yield complementary information. They characterize the extent to which the OH ground and excited states with $|\omega_A|=\frac{3}{2}$ and $\frac{1}{2}$ are mixed as well as the extent to which the populations of the $\pm\omega_A$ substates are perturbed by the interaction with HCl. The mixing occurs through the off-diagonal diabatic coupling potential $V_{1,-1}$. To better understand the role of this coupling we also present values of $\bar{\Lambda}$ calculated in the same way as $\bar{\omega}_A$. The quantity $\bar{\Lambda}$ is a measure for the extent to which the $\Lambda=\pm1$ components of $OH(^2\Pi)$ are mixed, i.e., for the amount of quenching of the OH orbital angular momentum in OH–HCl.

The bend quantum numbers $v_{b_{OH}}$, $v_{b_{HCl}}$, and the geometry indications "pl" and "npl" (planar and nonplanar) are obtained by analyzing the density distribution plots. Several of these plots are shown in Figs. 4–6. The density distributions were obtained by taking absolute squares of the rovibronic wave functions, summation over the electronic states, and integration over the overall rotation angles (α,β) of the complex. The radial coordinate was fixed at $R=6.6a_0$, which is slightly larger than the distance for the hydrogen-bonded equilibrium geometry of the complex. By combining the density distributions for the dihedral angle ϕ at $\phi=0°$ and $\phi=180°$ we show in Figs. 4 and 5 the density distributions for all planar geometries of the complex.

The rotational constant B_v of each state for the 4D model

TABLE II. Energies of lowest bound states of e parity and rotational constants B_v in cm^{-1} from 4D and (3+1)D calculations for $|\Omega|=\frac{3}{2}$. See Table I for explanation of the symbols.

State	$E_{J=3/2}$	Geometry	$\bar{\omega}_A$	$\langle\|\omega_A\|\rangle$	$\bar{\Lambda}$	v_s	$v_{b_{OH}}$	$v_{b_{HCl}}$	$E^{\sharp}_{J=3/2}$	$(\eta,v_s)^{\sharp}$	$B^{\sharp}_v$
1	−709.04	pl	−0.66	1.21	−0.36	0	0	0	−707.88	0,0	0.1249
2	−631.30	pl	0.31	1.16	0.04	0	0	0	−629.75	1,0	0.1264
3	−618.70	pl	−0.74	1.22	−0.41	1	0	0	−617.09	0,1	0.1212
4	−570.69	pl	−0.77	1.27	−0.47	0	1	0	−574.46	2,0	0.1244
5	−541.26	pl	0.01	1.22	−0.10	1	0	0	−538.38	1,1	0.1233
6	−536.02	npl	−0.56	1.17	−0.30	0	···	···	−529.11	3,0	0.1275
7	−531.50	npl	−0.54	1.17	−0.29	0*	···	···	−534.40	0,2	0.1178
8	−501.18	pl	0.40	1.17	0.11	0	2	0	−497.38	4,0	0.1272
9	−490.37	···	−0.46	1.23	−0.30	0*	···	···	−495.18	2,1	0.1234
10	−469.29	npl	−0.00	1.24	−0.08	0	···	···	−468.79	5,0	0.1264
11	−462.76	pl	−0.55	1.26	−0.36	···	···	···	−459.51	0,3	0.1150
12	−452.76	npl	−0.48	1.16	−0.24	1	···	···	−445.24	3,1	0.1235
13	−450.47	pl	−0.18	1.18	−0.15	2*	···	···	−456.15	1,2	0.1206
14	−440.08	pl	−0.46	1.10	−0.32	0	···	···	−439.79	6,0	0.1261
15	−442.42	pl	0.24	1.20	0.09	1	···	···	−414.86	4,1	0.1235
16	−414.78	npl	−0.11	1.18	−0.17	1	···	···	−389.87	5,1	0.1222
17	−409.06	npl	−0.41	1.17	−0.22	0	···	···	−406.24	7,0	0.1247

was calculated according to the formula $B_v=(E_{J=3/2}-E_{J=1/2})/3$. The latter was obtained from the approximate formula

$$E(J,|\Omega|) \approx E_0(|\Omega|) + B_v(|\Omega|)J(J+1), \tag{15}$$

where the energies $E(J,|\Omega|)$ are averaged over the e and f parities. The OH–HCl complex is a near symmetric top, hence Ω is a nearly good quantum number; consequently, Eq. (15) can be used for each $|\Omega|$. Within the framework of the (3+1)D model the rotational constants $B_v=\langle[2\mu_{AB}R^2]^{-1}\rangle$ were obtained by averaging over the 1D radial eigenfunctions composed of sinc-DVR basis functions. In the (η,v_s) abbreviation η labels the AB curves on which radial stretch states v_s were computed.

Table III lists the parity splittings $\Delta E=E_f-E_e$ for the 4D model and the 3D calculations. The parity splittings for the 4D model are shown for every given state. In order to compare the two models the 3D model parity splittings were computed with the intermolecular distance fixed at the equilibrium distance for the lowest AB potential, $R_e=6.4a_0$.

B. Interpretation and discussion

The lowest rovibronic state with $E=-723.12$ cm^{-1} possesses a planar geometry (see Fig. 6) located around $\theta_{OH}=110°$, $\theta_{ClH}=176°$ (see Fig. 4) and clearly corresponds to the global minimum with $D_e=1123$ cm^{-1} of the lowest adiabatic potential V_1 shown in Fig. 3. The dissociation energy of the

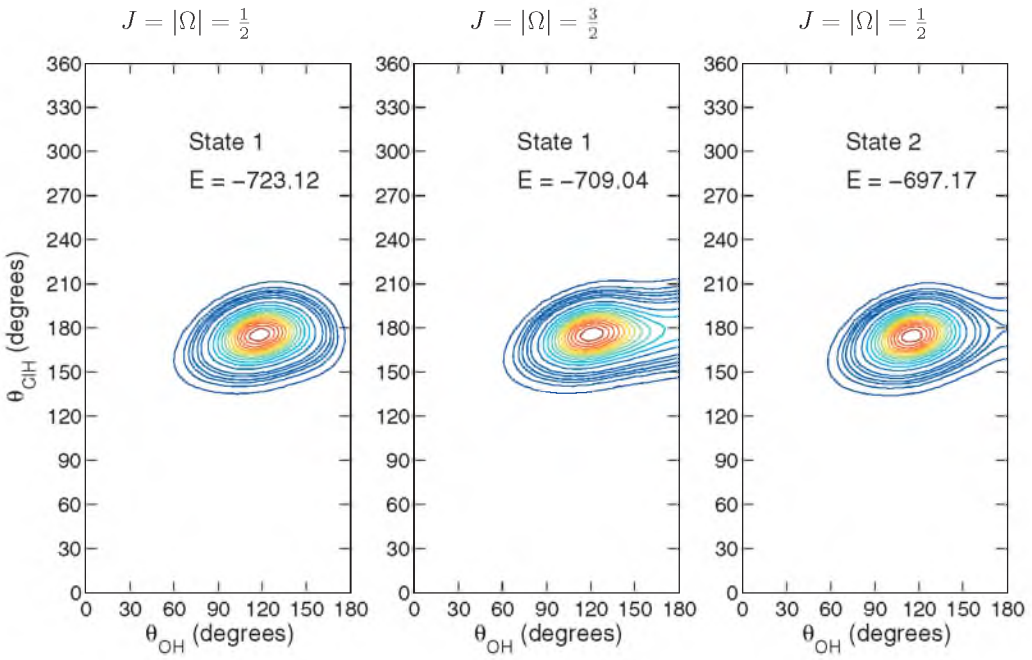

FIG. 4. Density distributions for planar geometries of the lowest states with $|\Omega|=\frac{1}{2}$ and $\frac{3}{2}$ from the 4D calculations.

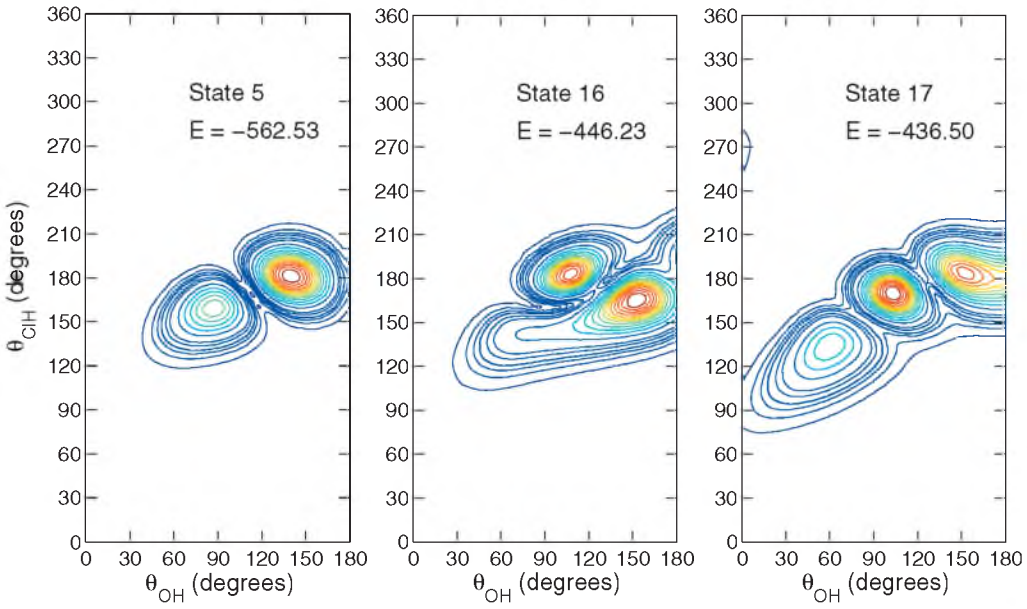

FIG. 5. Density distributions for planar geometries of some bend excited states from the 4D calculations for $J=|\Omega|=\frac{1}{2}$.

OH–HCl complex $D_0=684.9$ cm^{-1} is less than 723.12 cm^{-1} because the OH($^2\Pi_{3/2}$) ground state has an energy of −38.2 cm^{-1} on the energy scale used in our calculations. Only for states much higher in energy, as, for example, for state 17 with $E=-436.50$ cm^{-1} (see Fig. 5) the density distribution contours approach the local minimum of the V_1 potential seen in Fig. 3 at $\theta_{OH}=5.5°$ and $\theta_{ClH}=86.9°$.

For the lowest eight bound states for $J=\frac{1}{2}$ with $|\Omega|=\frac{1}{2}$ one can easily assign the approximate quantum numbers indicated in Table I. All eight states possess a planar geometry except state number 8 with $E=-532.94$ cm^{-1}, which is nonplanar and probably excited in the torsional mode, as one can see in Fig. 6.

The ground state ($E=-723.12$ cm^{-1}) has a mixed electronic character with populations of 53% of $\omega_A=-\frac{3}{2}$, 7% of $\omega_A=-\frac{1}{2}$, 27% of $\omega_A=\frac{1}{2}$, and 13% of $\omega_A=\frac{3}{2}$. State 3 has almost the same population distribution among the ω_A values. Such a similar electronic character might be expected because this state is the first stretch excited state. Also the angular density distribution of state 3 with $E=-629.54$ cm^{-1} looks almost the same as that of the ground state with $E=-723.12$ cm^{-1} in Fig. 4. The second stretch-excited state is state number 7. The electronic similarity of the three stretch states is nicely reflected by the very similar values of $\bar{\omega}_A$, $\langle|\omega_A|\rangle$, and $\bar{\Lambda}$ in Table I. The end-over-end rotational constant B_v for states 1, 3, and 7 is observed to decrease with increasing value of the stretch quantum number v_s as expected.

The lowest excited state for $|\Omega|=\frac{1}{2}$, state 2 with $E=-697.17$ cm^{-1}, is electronically excited and has the largest contributions from $\omega_A=\frac{3}{2}$ (48%) and $\omega_A=-\frac{1}{2}$ (31%). Hence, this state is the electronic counterpart of the ground state in the sense that it has nearly the same weights for opposite values of ω_A. One should remember that all the values of ω_A mentioned refer to the $\Omega>0$ components of the (parity-

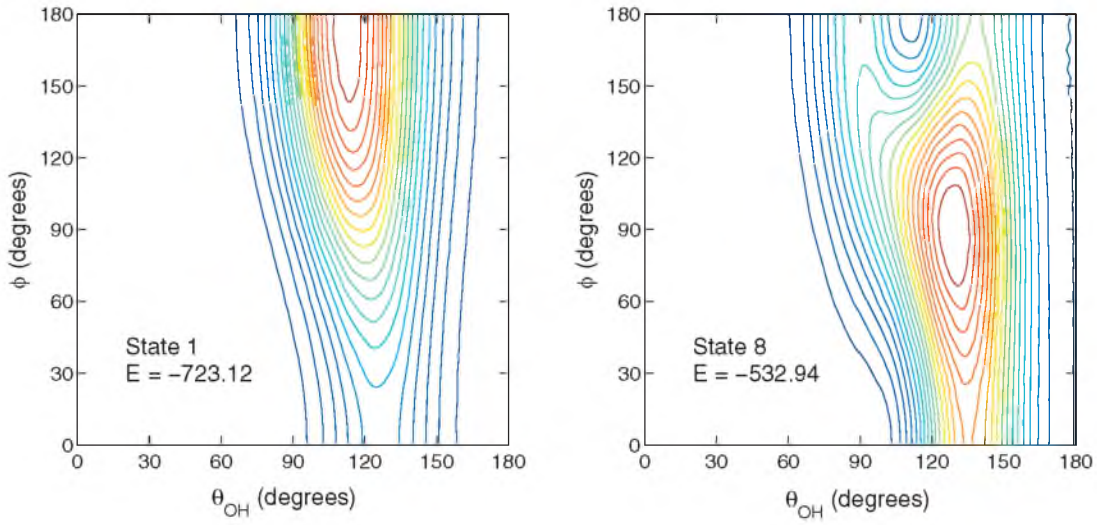

FIG. 6. Density distributions from 4D calculations for $J=\frac{1}{2}$ and $|\Omega|=\frac{1}{2}$ as functions of θ_{OH} and ϕ with $\theta_{HCl}=170.53°$ and $R=6.6a_0$.

TABLE III. Parity splittings $\Delta E=E_f-E_e$ in cm^{-1} from 4D calculations and 3D calculations with R fixed at $R_e=6.4a_0$ for $|\Omega|=\frac{1}{2}$. See Table I for explanation of the symbols; the 3D results are labeled with ♯ and η_e numbers the 3D energy levels, i.e., the AB curves at R_e.

State	$\Delta E_{J=1/2}$	$\Delta E_{J=3/2}$	Geometry	$\bar{\omega}_A$	$\langle\|\omega_A\|\rangle$	$\bar{\Lambda}$	v_s	$v_{b_{OH}}$	$v_{b_{HCl}}$	$\eta_e^\sharp$	$\Delta E^\sharp_{J=1/2}$	$\Delta E^\sharp_{J=3/2}$
1	−0.298	−0.595	pl	−0.51	1.16	−0.21	0	0	0	0	−0.301	−0.602
2	0.086	0.171	pl	0.38	1.13	0.09	0	0	0	1	0.083	0.167
3	−0.291	−0.582	pl	−0.55	1.17	−0.24	1	0	0			
4	0.091	0.183	pl	0.40	1.14	0.10	1	0	0			
5	−0.306	−0.612	pl	−0.40	1.20	−0.19	0	1	0	2	−0.313	−0.625
6	0.085	0.170	pl	−0.14	1.17	−0.09	0	1	0	3	0.076	0.153
7	−0.249	−0.492	pl	−0.55	1.19	−0.26	2^*	0	0			
8	0.239	0.478	npl	0.13	1.07	0.06	0	1	0	4	0.281	0.562
9	0.009	0.018	npl	0.24	1.09	0.01	0	⋯	⋯	5	−0.024	−0.049
10	0.063	0.125	pl	0.29	1.08	0.01	2^*	0	0			
11	−0.311	−0.621	pl	−0.39	1.22	−0.20	1	1	0			
12	0.158	0.317	npl	−0.25	1.18	−0.13	1	⋯	⋯			
13	−0.204	−0.408	npl	−0.54	1.20	−0.27	⋯	⋯	⋯			
14	0.019	0.063	npl	0.31	1.13	0.03	1	⋯	⋯			
15	0.109	0.195	npl	−0.11	1.08	−0.07	1^*	⋯	⋯			
16	−0.221	−0.441	pl	−0.74	1.27	−0.43	0	0	1	6	−0.300	−0.598
17	0.065	0.130	pl	0.58	1.18	0.24	0^*	2	0	7	0.042	0.084
18	0.039	0.077	pl	0.40	1.16	0.16	0^*	⋯	⋯			
19	−0.015	−0.028	pl	−0.80	1.24	−0.51	0	⋯	⋯	8	0.164	0.327
20	−0.033	−0.065	pl	0.34	1.21	0.15	0	⋯	⋯	9	−0.168	−0.337

adapted) eigenstates, the corresponding $\Omega<0$ components have the same weights for opposite values of ω_A. Qualitatively, the situation is the same for state 4 with $E=-603.58$ cm^{-1}, which is stretch excited with respect to state 2. The stretch excitation energy of 93.59 cm^{-1} is very similar to the energy difference of 93.58 cm^{-1} between the lowest stretch excited level, state 3, and the ground state. The strongly mixed ω_A character shows that the $|\omega_A|=\frac{1}{2}$ spin-orbit excited state of OH is heavily admixed into the spin-orbit ground state with $|\omega_A|=\frac{3}{2}$. Moreover, the populations of the substates with opposite values of ω_A become unequal. This mixing is a result of the coupling caused by the $V_{-1,1}=V^*_{1,-1}$ off-diagonal diabatic potential [cf. Eq. (9)], which mixes the diabatic states with $\Lambda=1$ and $\Lambda=-1$ and, thereby, the spin-orbit diabatic states $\omega_A=\frac{3}{2}$ with $\omega_A=-\frac{1}{2}$ and $\omega_A=-\frac{3}{2}$ with $\omega_A=\frac{1}{2}$. The strong diabatic coupling effect is reflected by the small value of $\bar{\Lambda}$ equal to 0.09, which indicates that the diabatic states with $\Lambda=-1$ and $\Lambda=1$ almost equally contribute to the bound states considered. In other words, the orbital angular momentum about the OH axis, which is $|\Lambda|=1$ in free OH, is nearly quenched in the complex.

In Fig. 4 one observes that the contour lines in the density distribution plot of state 2 with $E=-697.17$ cm^{-1} reach the $\theta_{OH}=180°$ border. Obviously, these states have a geometry closer to linear than the ground state (and its corresponding stretch-excited states). Comparing this with the contour lines of the higher adiabatic potential V_2 in Fig. 3, one observes that these low lying electronically excited states have considerable amplitude in the region of the global minimum in the V_2 potential. So it is clear that the second adiabatic state of the complex becomes relatively more important for these states than for the ground state.

State 5 with energy $E=-562.53$ cm^{-1} (160.6 cm^{-1} relative to the ground state) and $\omega_A=-\frac{3}{2}$ (50%), $\omega_A=-\frac{1}{2}$ (9%), $\omega_A=\frac{1}{2}$ (21%), and $\omega_A=\frac{3}{2}$ (20%) is bend excited, as shown in Fig. 5. The tilted nodal plane in the density distribution shows that this bend involves mostly the angle θ_{OH}, but to a considerable extent also the angle θ_{ClH}. The coupling between these two bend angles nicely reflects the shape of the potential well in the adiabatic potential V_1, see Fig. 3. So state 5 may be characterized as the (mostly) OH bend excited state. While state 6 is OH bend excited also, the ω_A population is a mixture of $\omega_A=-\frac{3}{2}$ (38%), $\omega_A=\frac{3}{2}$ (28%), and $\omega_A=\pm\frac{1}{2}$ (about 17% each). Here a considerable influence from the off-diagonal potential can also be seen, $\bar{\Lambda}=-0.09$. State 8 with $E=-532.94$ cm^{-1} is OH bend excited and possesses a nonplanar geometry with a strong diabatic coupling effect, $\bar{\Lambda}=0.06$. There are more states which are fully assigned in Table I in the same way as was done for the first eight states with $J=\frac{1}{2}$. Among the higher excited states we also found one, state 16 at $E=-446.23$ cm^{-1}, with a nodal plane nearly perpendicular to the nodal plane of the OH-bend excited state 5 with $E=-562.53$ cm^{-1}, see Fig. 5. So we may call this the HCl bend excited state, but one should remember that the OH and HCl bends are in fact strongly coupled.

The density distribution of the lowest state with $|\Omega|=\frac{3}{2}$ for $J=\frac{3}{2}$ is shown in Fig. 4. This state with $E=-709.04$ cm^{-1} in Table II has $\omega_A=-\frac{3}{2}$ (59%), $\omega_A=-\frac{1}{2}$ (9%), $\omega_A=\frac{1}{2}$ (21%), and $\omega_A=\frac{3}{2}$ (11%) and its first stretch excited state, state 3 with $E=-618.70$ cm^{-1}, has $\omega_A=-\frac{3}{2}$ (63%), $\omega_A=-\frac{1}{2}$ (8%), $\omega_A=\frac{1}{2}$ (19%), and $\omega_A=\frac{3}{2}$ (10%). As one can see from these population distributions, the effect of the off-diagonal diabatic coupling $V_{-1,1}$ is somewhat smaller for these states. This is confirmed by the expectation values $\bar{\Lambda}=-0.36$ and $\bar{\Lambda}=-0.41$. Although the most probable geometry of these states is close to the minimum of the lowest adiabatic potential V_1, they are much more strongly delocalized

toward a linear geometry ($\theta_{OH}=180°$) than the $|\Omega|=\frac{1}{2}$ states. Also the minimum of the second adiabatic potential V_2 occurs for this near-linear geometry, see Fig. 3. Several of these results indicate that neither the diabatic nor the adiabatic picture holds, and that the bound states of OH–HCl could not have been calculated reliably on a single PES.

Also for $|\Omega|=\frac{3}{2}$ a number of excited states could be identified. A rather low lying electronically excited state, state 2, occurs at -631.30 cm^{-1}, a stretch excited state, state 3, at -618.70 cm^{-1} (90.3 cm^{-1} relative to the lowest $|\Omega|=\frac{3}{2}$ state), and a bend excited state, state 4, at -570.69 cm^{-1} (152.4 cm^{-1} relative to the ground state).

According to Tables I and II the results from the (3+1)D model agree quite closely with the results from the full 4D model for the lowest rovibronic states for both $|\Omega|=\frac{1}{2}$ and $|\Omega|=\frac{3}{2}$. The rovibronic ground state corresponds to $J=\frac{1}{2}$ with energies $E=-723.12$ cm^{-1} and $E=-721.65$ cm^{-1} for the 4D and (3+1)D models, respectively. In addition, the rotational constants extracted from the two models in a rather different manner are quite consistent. The (3+1)D model was very helpful in assigning stretch quantum numbers for higher energy states in the 4D model. It should be mentioned that many of the (3+1)D energy levels match well with the levels of the 4D model; for higher energy states the match is not quantitative anymore, and at some point there is too much mixing. This mixing can already be expected from the occurrence of avoided crossings in the AB curves in Fig. 2.

The parity splittings of the levels with $J=\frac{1}{2}$ and $\frac{3}{2}$ are presented for $|\Omega|=\frac{1}{2}$ in Table III. The energy difference between functions with e and f parity is caused by a coupling between the basis components in Eq. (13) with Λ,ω_A,Ω and $-\Lambda,-\omega_A,-\Omega$. The shift terms $-(\hat{J}_{-AB}^{(DF)}\hat{J}_{-}^{(DF)}+\hat{J}_{+AB}^{(DF)}\hat{J}_{+}^{(DF)})/(2\mu_{AB}R^2)$ in the Coriolis operator in the Hamiltonian (1) are responsible for coupling $\Omega=\frac{1}{2}$ and $\Omega=-\frac{1}{2}$. These terms do not couple $\pm\Lambda$ and $\pm\omega_A$ components, but it should be noted that (as explained above) components with opposite signs of Λ and ω_A are present already in the $\Omega>0$ part of the eigenstate as well as in the $\Omega<0$ part. Therefore, the shift terms that couple $\Omega=\pm\frac{1}{2}$ also couple $|\Lambda,\omega_A,\Omega\rangle$ with $|-\Lambda,-\omega_A,-\Omega\rangle$. Given the form of the shift operators, the parity splittings should be proportional to $J+\frac{1}{2}$. The splittings for $J=\frac{3}{2}$ are indeed larger by a factor of 2 than the splittings for $J=\frac{1}{2}$. The parity splittings of the levels with $|\Omega|=\frac{3}{2}$ are very small on the order of 10^{-4} cm^{-1} or less and are not shown.

The parity splittings from the 4D model agree very well with the 3D calculations for the lowest states when R is fixed at $6.4a_0$. The discrepancy for the higher energy states can be explained by the avoided crossings between the AB bender curves, which lead to state swapping. Also the comparison of stretch and bend excitation frequencies from the (3+1)D model with the results of the 4D calculations indicates that the former provides a very useful approximation to the bound levels of the OH–HCl complex.

In order to understand better the role of the off-diagonal diabatic potential $V_{-1,1}$ and the way in which the spin-orbit coupling of OH is quenched we performed calculations in which the spin-orbit coupling constant A_0 is set to zero instead of its normal value $A_0=-139.21$ cm^{-1}. When A_0 is set to zero we also set the Λ-type doubling parameters p and q of OH to zero, so that the electron spin is completely decoupled from all other variables. These model calculations were carried out for $J=\frac{1}{2}$, $J=\frac{3}{2}$, and $J=\frac{5}{2}$ in the 3D model with R fixed at $6.4a_0$. In free OH the ground $(|\omega_A|=\frac{3}{2})$ and excited $(|\omega_A|=\frac{1}{2})$ spin-orbit states would be degenerate if spin-orbit coupling were switched off. The effect of the spin-orbit coupling term in free OH is to lower the $|\omega_A|=\frac{3}{2}$ state by 69.61 cm^{-1} and to raise the $|\omega_A|=\frac{1}{2}$ state by the same amount. The effect of the A_0 value on the lower levels of OH–HCl is shown in Fig. 7; the characteristics of the corresponding states are given in Table IV.

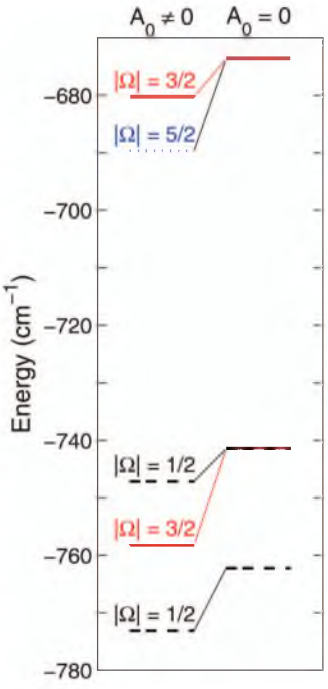

FIG. 7. Comparison of the 3D energy levels of parity e at $R=6.4a_0$ with and without spin-orbit coupling; dashed lines correspond to $J=|\Omega|=\frac{1}{2}$, closed lines to $J=|\Omega|=\frac{3}{2}$, and dotted lines to $J=|\Omega|=\frac{5}{2}$.

To understand the observed level pattern it is useful to discuss first the results for $A_0=0$ in which the spin is completely decoupled from all other variables. The level splittings are then caused by the anisotropic potential and, in particular, by the off-diagonal coupling potential $V_{-1,1}$. The ground state has a planar geometry, on average, with a rovibronic wave function of A'' symmetry that is antisymmetric under reflection in the plane of the equilibrium structure. As discussed above it is localized around the minimum of the lowest adiabatic potential V_1. The corresponding adiabatic electronic state of A'' symmetry is an antisymmetric linear combination of the diabatic states with $\Lambda=+1$ and -1. The corresponding symmetric state of A' symmetry is associated with the second adiabatic potential V_2. Since the minimum of the latter potential is higher than the minimum in V_1 by 266 cm^{-1} it is expected that this state is higher than the ground state by about this amount. The large splitting between these two electronic states is caused by the diabatic coupling potential $V_{-1,1}$. Since this splitting is so large, the lower rovibronic states of OH–HCl can be considered in first

TABLE IV. Energies of states with parity e in cm^{-1} shown in Fig. 7 and electronic quantum numbers from 3D calculations at $R=6.4a_0$ with and without spin-orbit coupling included.

	$A_0=-139.21$ cm^{-1}				$A_0=0$			
J	E	$\bar{\omega}_A$	$\langle\lvert\omega_A\rvert\rangle$	$\bar{\Lambda}$	E	$\bar{\omega}_A$	$\langle\lvert\omega_A\rvert\rangle$	$\bar{\Lambda}$
				$\lvert\Omega\rvert=\frac{1}{2}$				
$\frac{1}{2}$	−773.12	−0.49	1.15	−0.20	−762.20	−0.19	1.00	−0.00
$\frac{3}{2}$	−772.59	−0.50	1.15	−0.20	−761.70	−0.19	1.00	−0.00
$\frac{5}{2}$	−771.82	−0.50	1.15	−0.20	−760.94	−0.19	1.00	−0.00
$\frac{1}{2}$	−747.13	0.37	1.12	0.08	−741.42	0.05	0.96	−0.14
$\frac{3}{2}$	−746.79	0.37	1.12	0.08	−740.92	−0.04	0.98	−0.14
$\frac{5}{2}$	−746.20	0.37	1.12	0.09	−740.17	−0.07	0.99	−0.14
				$\lvert\Omega\rvert=\frac{3}{2}$				
$\frac{3}{2}$	−758.21	−0.63	1.20	−0.33	−741.42	−0.23	1.02	−0.14
$\frac{5}{2}$	−757.59	−0.63	1.20	−0.33	−740.92	−0.20	1.02	−0.14
$\frac{7}{2}$	−680.29	0.30	1.14	0.04	−673.60	−0.00	0.95	−0.16
$\frac{9}{2}$	−679.65	0.30	1.14	0.04	−672.85	−0.06	0.97	−0.16
				$\lvert\Omega\rvert=\frac{5}{2}$				
$\frac{5}{2}$	−689.68	−0.56	1.18	−0.31	−673.60	−0.27	1.03	−0.16

approximation as if the complex has only a single electronic (adiabatic) state. It has a bent geometry with OH making an angle θ_{OH} of about 110° with the intermolecular axis and HCl nearly aligned with this axis. Such a geometry corresponds to a near-symmetric rotor and the rotational states can be labeled with the quantum number K, the projection of the total angular momentum J (without spin) on the dimer z-axis. The ground state has $K=0$, then there are two states with $K=\pm 1$ that are only slightly split by a small asymmetry doubling, next two nearly degenerate states with $K=\pm 2$, etc. The $K=\pm 1$ states have an energy A with respect to the ground $K=0$ state, the $K=\pm 2$ states have an energy $4A$, where A is the rotational constant of the prolate near-symmetric rotor associated with rotation around the long axis. If one looks at the levels calculated for $A_0=0$ in Fig. 7 one finds that such an energy pattern is indeed observed with a value of A of about 21 cm^{-1}. This value is close to the value calculated for OH–HCl in its equilibrium geometry. Spin has not been considered so far, but since for $A_0=p=q=0$ the spin is completely free, one can simply include the spin without affecting the energies. Since $S=\frac{1}{2}$ the values $\pm\frac{1}{2}$ of the spin projection on the dimer axis must be added to the values of K to obtain the values of Ω as defined in our calculations. For $K=0$ one obtains $\Omega=\pm\frac{1}{2}$, for $K=\pm 1$ one gets $\Omega=\pm\frac{1}{2}$ and $\Omega=\pm\frac{3}{2}$, for $K=\pm 2$ one gets $\Omega=\pm\frac{3}{2}$ and $\Omega=\pm\frac{5}{2}$, etc. This splitting pattern and the corresponding quantum numbers are in perfect agreement with the energy levels shown at the right hand side of Fig. 7 and tabulated for $A_0=0$ in Table IV.

Let us now switch on spin-orbit coupling with $A_0=-139.21$ cm^{-1}, as in the full 4D calculations. The spin-orbit coupling operator mixes the ground electronic state, which is an antisymmetric combination of the OH substates with $\Lambda=+1$ and -1 with the excited state that corresponds to the symmetric combination and, thereby, unquenches the angular momentum Λ. Since these electronic states are split by nearly 300 cm^{-1} through the effect of $V_{-1,1}$ this mixing will only occur to a limited extent. The fact that indeed the orbital angular momentum Λ stays nearly quenched can be seen from the values of $\bar{\Lambda}$ in Table IV. It can also be concluded from the rather small splitting of the levels with $K=\pm 1$ and $K=\pm 2$ that were degenerate when $A_0=0$ and from the small energy lowering (about 11 cm^{-1}) of the levels obtained when A_0 is set to -139.21 cm^{-1}. The nearly degenerate (spin-free) level with $K=\pm 1$ splits into a level with $\Omega=\pm\frac{3}{2}$ at 15 cm^{-1} above the ground level and a level with $\Omega=\pm\frac{1}{2}$ at 26 cm^{-1}. The level with $K=\pm 2$ splits into a level with $\Omega=\pm\frac{5}{2}$ at 83 cm^{-1} above the ground level and a level with $\Omega=\pm\frac{3}{2}$ at 93 cm^{-1}. All levels shown originate from the lower spin-free state (of A'' symmetry) and are lowered in energy with respect to their spin-free counterparts. This is because the spin-free states of A' and A'' symmetries are symmetric and antisymmetric combinations of the states with $\Lambda=+1$ and -1, and the orbital angular momentum operator L_z has only an off-diagonal matrix element between the spin-free states. All the lower levels contain somewhat more of the OH spin-orbit ground state with $\lvert\omega_A\rvert=\frac{3}{2}$ than of the excited spin-orbit state with $\lvert\omega_A\rvert=\frac{1}{2}$, hence, all the values of $\langle\lvert\omega_A\rvert\rangle$ in Table IV are larger than 1. Levels that have predominantly $\lvert\omega_A\rvert=\frac{1}{2}$ character will be found in the region of the excited electronic state with an energy of about 300 cm^{-1}, but it might be difficult to identify such levels because there are several bend and stretch excited states of the complex in the same energy region that will all be mixed. In summary, we may conclude from this discussion that the energy level pattern for the lower states of the OH–HCl complex can be completely understood. It is in first instance dominated by the large off-diagonal coupling potential $V_{-1,1}$ that quenches the orbital angular momentum Λ of the $OH(^2\Pi)$ state and gives rise to a large splitting of the electronic states. Spin-orbit coupling partly unquenches the elec-

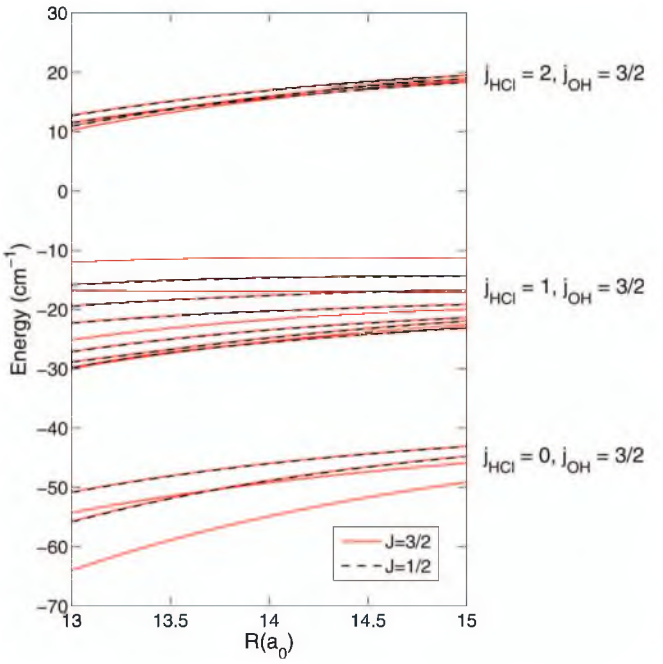

FIG. 8. The AB potentials at long distance range.

tronic orbital angular momentum and gives further (smaller) splittings and an overall energy lowering of the lower levels.

To provide further help with the interpretation of the states, the AB potentials were calculated in the 3D model for values of R up to $15a_0$. At this distance, the intermolecular forces are very weak and dominated by the dipole-dipole interaction proportional to R^{-3}. The OH and HCl constituents start to behave as if they are free molecules and the AB energy curves can be labeled with the quantum numbers of free OH and HCl, see Fig. 8. The index η_{lr} given in Table V labels the curves plotted in Fig. 8 in increasing energy order, while the index η_e refers to the energy order of the 3D bound levels at the equilibrium distance $R_e=6.4a_0$, see Fig. 2. This value of R_e corresponds to the minimum in the lowest AB curves.

As one can see in Fig. 8 the AB energy levels appear in groups. The curves within each group converge to specific rotational levels of HCl and OH. It is seen in the figure that the energy differences between the $j_{\mathrm{HCl}}=0$ and $j_{\mathrm{HCl}}=1$ curves and between the $j_{\mathrm{HCl}}=1$ and $j_{\mathrm{HCl}}=2$ groups start approaching the asymptotic values $2B_{0_{\mathrm{HCl}}}=20.88$ cm^{-1} and $4B_{0_{\mathrm{HCl}}}=41.76$ cm^{-1}, respectively. For all curves shown the OH fragment is in its ground spin-orbit state $^2\Pi_{3/2}$ with $j_{\mathrm{OH}}=\frac{3}{2}$. Higher OH levels are not shown in this figure because the energy difference between the ground $\left(j_{\mathrm{OH}}=\frac{3}{2}\right)$ and the lowest excited $\left(j_{\mathrm{OH}}=\frac{5}{2}\right)$ OH rotational level is 84 cm^{-1} and the $^2\Pi_{1/2}$ excited spin-orbit state is separated in energy from the ground $^2\Pi_{3/2}$ state by 126 cm^{-1}. As the number of crossings between $j_{\mathrm{HCl}}=0$ and $j_{\mathrm{HCl}}=1$ curves is limited, it is still possible to label the curves at $R_e=6.4a_0$ with the quantum number j_{HCl}.

In Table V each of the asymptotic states is not only labeled with the rotational quantum numbers of the OH radical (A) and the HCl molecule (B) but also with the quantum number l that characterizes the end-over-end rotation of the complex in the SF frame. This quantum number corresponds to the angular momentum operator $\hat{\mathbf{l}}^{(\mathrm{SF})}=\hat{\mathbf{J}}^{(\mathrm{SF})}-\hat{\mathbf{j}}_{AB}^{(\mathrm{SF})}$ and its

TABLE V. Long range state ordering and quantum numbers from 3D calculations and correlation with the 3D levels calculated at $R_e=6.4a_0$.

			$J=\frac{1}{2}$		$J=\frac{3}{2}$					
j_{OH}	j_{HCl}	j_{AB}	l	Ω	l	Ω	η_{lr}	η_e	J	Ω
$\frac{3}{2}$	0	$\frac{3}{2}$	1,2	$\pm\frac{1}{2}$	0,1,2,3	$\pm\frac{1}{2}$, $\pm\frac{3}{2}$	1	3	$\frac{3}{2}$	$\frac{3}{2}$
							2	6	$\frac{3}{2}$	$\frac{3}{2}$
							3	1	$\frac{1}{2}$	$\frac{1}{2}$
							4	2	$\frac{3}{2}$	$\frac{1}{2}$
							5	5	$\frac{1}{2}$	$\frac{1}{2}$
							6	4	$\frac{3}{2}$	$\frac{1}{2}$
$\frac{3}{2}$	1	$\frac{1}{2}$	0,1	$\pm\frac{1}{2}$	1, 2	$\pm\frac{1}{2}$	7	22	$\frac{1}{2}$	$\frac{1}{2}$
		$\frac{3}{2}$	1,2	$\pm\frac{1}{2}$	0,1,2,3	$\pm\frac{1}{2}$, $\pm\frac{3}{2}$	8	26	$\frac{3}{2}$	$\frac{3}{2}$
		$\frac{5}{2}$	2,3	$\pm\frac{1}{2}$	1,2,3,4	$\pm\frac{1}{2}$, $\pm\frac{3}{2}$	9	9	$\frac{3}{2}$	$\frac{1}{2}$
							10	10	$\frac{1}{2}$	$\frac{1}{2}$
							11	7	$\frac{3}{2}$	$\frac{3}{2}$
							12	8	$\frac{1}{2}$	$\frac{1}{2}$
							13	11	$\frac{3}{2}$	$\frac{1}{2}$
							14	20	$\frac{3}{2}$	$\frac{1}{2}$
							15	13	$\frac{1}{2}$	$\frac{1}{2}$
							16	14	$\frac{3}{2}$	$\frac{1}{2}$
							17	25	$\frac{3}{2}$	$\frac{1}{2}$
							18	30	$\frac{1}{2}$	$\frac{1}{2}$
							19	18	$\frac{3}{2}$	$\frac{3}{2}$
							20	15	$\frac{1}{2}$	$\frac{1}{2}$
							21	16	$\frac{3}{2}$	$\frac{1}{2}$
							22	12	$\frac{3}{2}$	$\frac{3}{2}$

possible values are determined by the triangular condition $|J-j_{AB}| \leq l \leq J+j_{AB}$. In the distance range displayed in Fig. 8 the end-over-end angular momentum l is not yet a good quantum number, but Table V explains in detail how the AB levels correlate with the asymptotic states in the long range.

Unfortunately, no spectroscopic data for OH–HCl have been obtained yet that could be used to check the accuracy of our bound state results. Such data have been measured for OH–N_2, OH–CO, and OH-acetylene,[19–21] but the binding in these complexes is considerably weaker than in OH–HCl and their equilibrium geometries correspond to a hydrogen bonded structure with OH as the donor, whereas the bound states that we found and analyzed for OH–HCl are hydrogen bonded with HCl as the donor and OH as the acceptor. Another difference with OH–HCl is that the equilibrium geometries of OH–N_2 and OH–CO are linear and, therefore, that the orbital angular momentum Λ of OH is not quenched at all. The lowest bend fundamental frequencies found for OH–N_2 and OH–CO are 35.9 and 54.1 cm^{-1}, respectively, while we obtained 160 cm^{-1} for OH–HCl. This is in agreement with the binding and the anisotropy of the potential in OH–N_2 and OH–CO being considerably weaker than in OH–HCl. The theoretical model that was developed in Refs. 19 and 20 is to some extent similar to the methods used in the present paper, but it involves only the angular (monomer bend) coordinates and the $\omega_A = \pm\frac{3}{2}$ spin-orbit ground state of OH. The dipole-quadrupole model used for the OH–N_2 potential does not contain the off-diagonal—or difference, see Eq. (8)—potential $V_{1,-1}$ that has such important effects in OH–HCl. For OH–CO a quadrupole-quadrupole interaction term was added, which gives a difference potential, but the effect of this difference potential seems to be much smaller than we found for OH–HCl. The OH-acetylene complex is T-shaped and the OH orbital momentum is partly quenched, as in OH–HCl. The theoretical model[21] used to analyze the spectra of this complex assumes a rigid T-shaped (hence, planar) structure with OH fixed along the twofold symmetry axis, very different from the models by which we treated OH–HCl.

We may also compare our results for the OH–HCl complex to the theoretical results of Yu and Nyman[15] already mentioned in Sec. I of this paper. They employed, however, quite different theoretical methods than we did and their calculations are based on a single PES only. They used second-order Møller–Plesset perturbation theory with the 6-311G(2*d*,*d*,*p*) basis set, which is rather small for this system. Unlike the work described here, Yu and Nyman did not apply the basis set superposition error correction in their electronic structure calculations but instead used a scaling method. They obtained a binding energy $D_e = 1910$ cm^{-1}, whereas we find $D_e = 1123$ cm^{-1}. They also estimated the dissociation energy D_0 from the equation $D_0 = D_e - \mathcal{E}_{0_{\text{complex}}} + \mathcal{E}_{0_{\text{fragments}}} = 1473$ cm^{-1}, where $\mathcal{E}_0$ is the zero point vibrational energy computed in the harmonic approximation. The value of Yu and Nyman for the zero point vibrational energy is 437 cm^{-1}; from our value of $D_0 = 685$ cm^{-1} we obtained 438 cm^{-1}. The value of Yu and Nyman[15] takes into account the zero point energy of all normal modes, however, while our value only includes the intermolecular modes. Moreover, our value includes spin-orbit coupling effects, the value of Yu and Nyman does not. They also calculated the intermolecular (harmonic) stretch fundamental frequency $\nu_s = 135$ cm^{-1}, while according to our fully anharmonic results $\nu_s = 93.6$ cm^{-1}.

V. SUMMARY AND CONCLUSIONS

Bound states of the open-shell OH–HCl complex were computed in four dimensions with rigid monomers. The intermolecular interaction in the complex is described by a 2×2 matrix of diabatic potentials taken from Ref. 18. Bound state calculations were carried out for $J = \frac{1}{2}$ and $J = \frac{3}{2}$ in a full 4D approach and with the use of a (3+1)D model that adiabatically separates the electronic and angular motions from the radial motion. Spin-orbit coupling was included. The bound states calculated in the 4D model were analyzed by computing various approximate quantum numbers, as well as geometric density distributions of a number of low lying states, and with some help from the (3+1)D model.

The ground state of the complex with $J = |\Omega| = \frac{1}{2}$ turned out to have a planar geometry and a dissociation energy of $D_0 = 685$ cm^{-1} obtained from the 4D model. This may be compared to the binding energy $D_e = 1123$ cm^{-1} corresponding to the minimum in the lowest adiabatic potential. The rotational constants from the 4D calculations and the parity splittings were calculated from the usual spectroscopic fits of the levels for the different J values; in the (3+1)D model the rotational constants were obtained from expectation values. Fully anharmonic values for the fundamental frequencies were computed to be 94 cm^{-1} for the HO–HCl hydrogen-bond stretch and about 160 cm^{-1} for the bend. The latter involves a coupled bend motion of both fragments.

Although we have not performed calculations on the two adiabatic potentials separately it is clear from the results that nonadiabatic coupling effects are important, especially for the excited states. In the 2×2 diabatic model used, the off-diagonal diabatic coupling potential is responsible for quenching most of the orbital angular momentum of OH and, hence, for a strong reduction in the spin-orbit coupling that causes the splitting between the $^2\Pi_{3/2}$ and $^2\Pi_{1/2}$ states in free OH. Low lying rovibronic states correlating with the OH($^2\Pi_{3/2}$) ground state were found at 14 cm^{-1} above the ground state for $|\Omega| = \frac{3}{2}$ and at 26 cm^{-1} for $|\Omega| = \frac{1}{2}$.

We could assign monomer rotational quantum numbers to the bound states of the complex calculated at large values of R with the help of our 3D model. For the lower states there are only a few crossings between the energy level curves plotted as functions of R, so we could even correlate the OH–HCl states computed at the equilibrium distance R_e to the separate fragment states. For higher energies the individual monomer states are fully mixed.

Lester and co-workers[19–21] (University of Pennsylvania) already measured rotationally resolved infrared spectra of several OH-linear molecule complexes in a molecular beam setup and are trying to obtain the spectra for the OH–HCl complex.[36] The comparison of our results with these data will be a very good check of the reliability of the models employed and the quality of the potentials calculated by

Wormer *et al.* Inelastic OH–HCl scattering cross sections were measured by Cireasa *et al.*,[11,12] so it will also be useful to perform scattering calculations. The approach used for the bound state calculations presented here is similar to a coupled-channel scattering calculation, so it will be possible to use a large part of the formalism and of the code developed.

[1] R. P. Wayne, *An Introduction to the Chemistry of the Atmospheres of Earth, the Planets, and their Satellites* (Oxford University Press, New York, 1991).
[2] J. Warnatz, U. Maas, and R. W. Dibble, *Combustion: Physical and Chemical Fundamentals, Modeling and Simulation, Experiments; Pollutant Formation* (Springer-Verlag, Berlin, 1996).
[3] M. J. Molina, L. T. Molina, and C. A. Smith, Int. J. Chem. Kinet. **16**, 1151 (1984).
[4] L. F. Keyser, J. Phys. Chem. **88**, 4750 (1984).
[5] D. Husain, J. M. C. Plane, and C. C. Xiang, J. Chem. Soc., Faraday Trans. 2 **80**, 713 (1984).
[6] A. R. Ravishankara, P. Wine, J. R. Wells, and R. L. Thomson, Int. J. Chem. Kinet. **17**, 1281 (1985).
[7] I. W. M. Smith and M. D. Williams, J. Chem. Soc., Faraday Trans. 2 **82**, 1043 (1986).
[8] P. Sharkey and I. W. M. Smith, J. Chem. Soc., Faraday Trans. **89**, 631 (1993).
[9] F. Battin-Leclerc, I. K. Kim, R. K. Talukdar, R. W. Portmann, A. R. Ravishankara, R. Steckler, and D. Brown, J. Phys. Chem. A **103**, 3237 (1999).
[10] N. I. Butkovskaya and D. W. Setser, J. Chem. Phys. **108**, 2434 (1998).
[11] R. Cireasa, M. C. van Beek, A. Moise, and J. J. ter Meulen, J. Chem. Phys. **122**, 074319 (2005).
[12] R. Cireasa, A. Moise, and J. J. ter Meulen, J. Chem. Phys. **123**, 064310 (2005).
[13] D. C. Clary, G. Nyman, and E. Hernandez, J. Chem. Phys. **101**, 3704 (1994).
[14] R. Steckler, G. M. Thurman, J. D. Watts, and R. J. Bartlett, J. Chem. Phys. **106**, 3926 (1997).
[15] H.-G. Yu and G. Nyman, J. Chem. Phys. **113**, 8936 (2000).
[16] A. Rodriguez, E. Garcia, M. L. Hernández, and A. Laganà, Chem. Phys. Lett. **360**, 304 (2002).
[17] A. Rodriguez, E. Garcia, M. L. Hernández, and A. Laganà, Chem. Phys. Lett. **371**, 223 (2003).
[18] P. E. S. Wormer, J. Kłos, G. C. Groenenboom, and A. van der Avoird, J. Chem. Phys. **122**, 244325 (2005).
[19] M. D. Marshall, B. V. Pond, S. M. Hopman, and M. I. Lester, J. Chem. Phys. **114**, 7001 (2001).
[20] M. D. Marshall, B. V. Pond, and M. I. Lester, J. Chem. Phys. **118**, 1196 (2003).
[21] M. D. Marshall and M. I. Lester, J. Chem. Phys. **121**, 3019 (2004).
[22] A. Degli Esposti and H.-J. Werner, J. Chem. Phys. **93**, 3351 (1990).
[23] J. Kłos, G. Chałasiński, M. T. Berry, R. A. Kendall, R. Burcl, M. M. Szczęśniak, and S. M. Cybulski, J. Chem. Phys. **112**, 4952 (2000).
[24] G. Herzberg, *Molecular Spectra and Molecular Structure: Spectra of Diatomic Molecules*, (Van Nostrand, Princeton, 1950), Vol. 1.
[25] L. C. Biedenharn and J. D. Louck, *Angular Momentum in Quantum Physics*, Encyclopedia of Mathematics Vol. 8 (Addison-Wesley, Reading, MA, 1981).
[26] K. P. Huber and G. Herzberg, *Molecular Spectra and Molecular Structure. IV. Constants of Diatomic Molecules* (Van Nostrand Reinhold, New York, 1979).
[27] D. M. Brink and G. R. Satchler, *Angular Momentum*, 3rd ed. (Clarendon, Oxford, 1993).
[28] A. R. Offer and M. C. van Hemert, J. Chem. Phys. **99**, 3836 (1993).
[29] A. R. Offer, M. C. van Hemert, and E. F. van Dishoeck, J. Chem. Phys. **100**, 362 (1994).
[30] G. C. Groenenboom and D. T. Colbert, J. Chem. Phys. **99**, 9681 (1993).
[31] A. V. Fishchuk, Ph.D. thesis, Radboud University Nijmegen, 2008.
[32] E. R. Davidson, J. Comput. Phys. **17**, 87 (1975).
[33] G. C. Groenenboom, P. E. S. Wormer, A. van der Avoird, E. M. Mas, R. Bukowski, and K. Szalewicz, J. Chem. Phys. **113**, 6702 (2000).
[34] S. L. Holmgren, M. Waldman, and W. Klemperer, J. Chem. Phys. **67**, 4414 (1977).
[35] M. H. Alexander, S. Gregurick, and P. Dagdigian, J. Chem. Phys. **101**, 2887 (1994).
[36] M. I. Lester, private communication (2009).